System size effects and momentum correlations in heavy-ion collisions

Jatinder K. Dhawan and Rajeev K. Puri
Physics Department, Panjab University, Chandigarh-160 014, India
(Received 26 September 2006; published 9 May 2007)

We aim to carry out the detailed study of system-size effects and momentum correlations by simulating the reactions of ^{12}C+^{12}C, ^{20}Ne+^{20}Ne, ^{40}Ca+^{40}Ca, ^{58}Ni+^{58}Ni,^{93}Nb+^{93}Nb, ^{129}Xe+^{118}Sn, ^{139}La+^{139}La, and ^{197}Au+^{197}Au at an incident energy of 400 MeV/nucleon and over entire colliding geometry from a central to an extreme peripheral one. A mass-independent role of the momentum correlations is reported for the entire periodic table. When averaged over all fragments, the effect of momentum correlations for central collisions is about 39%. All mass yields can be parametrized by a power law with $2 \leqslant \tau \leqslant 3$ which is in agreement with other theoretical and experimental studies.

DOI: 10.1103/PhysRevC.75.057901 PACS number(s): 25.70.−z

Heavy-ion collisions at intermediate energies provide a unique possibility to study several rare phenomena. Among these, multifragmentation has an edge since it gives the first-hand information about the mutual interactions, fluctuations as well as correlations among nucleons [1]. The spatial and momentum correlations among nucleons of colliding nuclei have a significant role in the formation of fragments and their pattern [1,2]. In addition, the system-size dependence has always attracted a lot of attention. Whether, it is a fusion-fission, cluster-radioactivity, and structural physics at low incident energies or collective transverse flow, nuclear stopping, multifragmentation, and particle production at intermediate incident energies, the size of the system has been reported to influence the reaction dynamics from a mild to strong manner [3–7]. We here aim to study the role of momentum correlations in fragmentation for system-size effects and also the power law behaviors in multifragmentation which has also been thought to be a candidate for liquid-gas phase transition.

The aim of the present report is at least twofold: (i) It was pointed out by Curtin *et al.* [8] that the excited nuclear matter will pass through a liquid-gas phase transition stage at some incident energy, and if fragments are formed at this stage, these may show some characteristics of the liquid-gas phase transition [8,9]. In the last years, a large number of attempts have been made to fit the mass (or charge) yields with power laws (either $\propto A^{-\tau}$ or $e^{-\lambda A}$) and extract information about the possible liquid-gas phase transition in terms of the Fisher droplet model, which suggests a critical behavior for $2 \leqslant \tau \leqslant 3$ [10]. Interestingly, some studies [11], advocated minima in τ with variation in the incident energy whereas others denied [12]. Even, an accidental occurrence of power law behavior in multifragmentation was also advocated in some theoretical studies [13]. Most of the above studies concentrated on the analysis of mass (charge yields) as a function of incident energy [1,11,13]. Very little attention has been paid in the literature for the above power law dependence in terms of colliding geometry, i.e., in terms of impact parameters [11,14]. It is worth mentioning that these observations differ for different colliding nuclei. Therefore, it is of interest to study the power law dependence for system-size effects and also to understand whether momentum correlations have any role to play or not.

(ii) Recently, we reported an improvement over the spatial correlation method used to construct the fragments by imposing an additional momentum cut [15]. The first results for ^{197}Au+^{197}Au reactions demanded a detailed analysis over a larger mass range. We shall also present the system-size effects in the multiplicities of various fragments in terms of momentum correlations.

The present study is carried out within the framework of quantum molecular dynamics (QMD) model [1]. This is based on a molecular dynamics picture where nucleons interact via two- and three-body interactions. Here each nucleon α is represented by a Gaussian wave packet with a width of $\sqrt{L}$ centered around the mean position $\vec{r}_\alpha(t)$ and mean momentum $\vec{p}_\alpha(t)$ [1]. The centroid of each wave packet is propagated using the classical equations of motion [1]:

$$\frac{d\vec{r}_\alpha}{dt} = \frac{dH}{d\vec{p}_\alpha}, \tag{1}$$

$$\frac{d\vec{p}_\alpha}{dt} = -\frac{dH}{d\vec{r}_\alpha}, \tag{2}$$

where the Hamiltonian H is given by

$$H = \sum_\alpha \frac{\vec{p}_\alpha^{\,2}}{2m_\alpha} + V^{tot}. \tag{3}$$

Our total interaction potential V^{tot} reads as

$$V^{tot} = V^{loc} + V^{Yuk} + V^{Coul}, \tag{4}$$

The static (local) Skyrme interaction can further be parametrized as

$$U^{loc} = \alpha\left(\frac{\rho}{\rho_o}\right) + \beta\left(\frac{\rho}{\rho_o}\right)^\gamma. \tag{5}$$

Here α, β and γ are the parameters that define a equation of state.

In the present study, we shall use a soft equation of state with a standard energy dependent nucleon-nucleon cross section. As noted in Ref. [16], the different equations of state do not affect the conclusions of multifragmentation.

For the present analysis, we simulated the reactions of ^{12}C+^{12}C, ^{20}Ne+^{20}Ne, ^{40}Ca+^{40}Ca, ^{58}Ni+^{58}Ni, ^{93}Nb+^{93}Nb, ^{129}Xe+^{118}Sn, ^{139}La+^{139}La, and ^{197}Au+^{197}Au at an incident

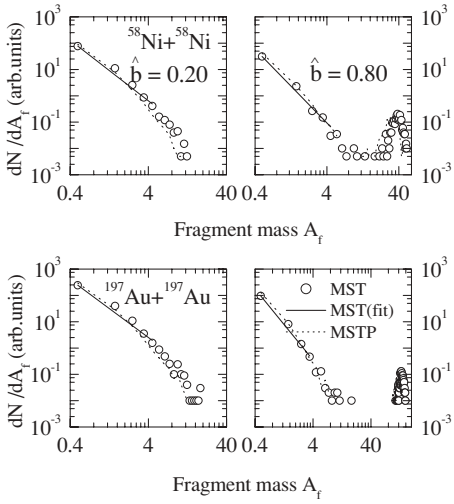

FIG. 1. The mass yield curves, i.e., dN/dA_f vs fragment mass (A_f) are displayed for the reactions of ^{58}Ni+^{58}Ni and ^{197}Au+^{197}Au at $\hat{b}$ = 0.2 and 0.8, respectively. The power law fits for MST results are shown by solid lines.

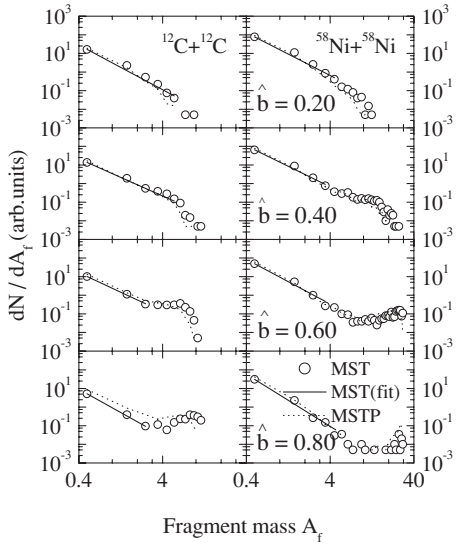

FIG. 2. The mass yield curves, i.e., dN/dA_f as a function of mass of fragments ($A_j \leqslant 30$) are displayed for the reactions of ^{12}C+^{12}C and ^{58}Ni+^{58}Ni at $\hat{b} = 0.2$, 0.4, 0.6, and 0.8, respectively. The power law fitting for the MST results is shown by solid lines.

energy of 400 MeV/nucleon and over an entire impact parameter $\hat{b} = b/b_{max}$ ranging from 0 to 0.8, with b_{max} equal to $R_P + R_T$ (R_P and R_T are the radii of projectile and target, respectively). The phase-space, thus, generated is then subjected to clusterization using a minimum spanning tree (or spatial correlations) MST method. In this method, two nucleons share the same fragment if they are closer than 4 fm, i.e., $|\vec{r}_\alpha - \vec{r}_\beta| \leqslant 4$ fm. In the extended version [15], we also imposed a restriction in the momentum space of the scattered nucleons. Now, nucleons should also obey $|\vec{p}_\alpha - \vec{p}_\beta| \leqslant p_{fermi}^{mean}$; p_{fermi}^{mean} is the mean Fermi momentum of nucleons, which in our case is 150 MeV/c. This is dubbed as the minimum spanning tree (P), i.e., MSTP method.

In Fig. 1, we display the mass yield dN/dA_f as a function of the mass of the fragments for ^{58}Ni+^{58}Ni and ^{197}Au+^{197}Au reactions at 400 MeV/nucleon and $\hat{b} = 0.2$ and 0.8, respectively. We see a single continuous curve with negative slope in central collisions whereas it starts following a U-shape with a peak at heavier fission products for peripheral collisions. The inclusion of momentum correlations in central collisions leads to a downsizing of all medium mass fragments. In contrary, heavier fragments break into intermediate mass fragments as well as into light mass fragments and free nucleons in peripheral collisions. The trend, interestingly, is independent of system size. The momentum correlations influence the mass yield uniformly throughout the periodic table. It is also evident that the effect of momentum correlations depend upon the excitation energy and density of the colliding nuclei. If the system is mildly excited, a larger effect can be seen whereas for highly excited matter the effect is nearly insignificant.

In Fig. 2, we display the mass yield (dN/dA_f) as a function of the mass of the fragments ($A_j \leqslant 30$) for $\hat{b}$ = 0.2 to 0.8 for the reactions of ^{12}C+^{12}C and ^{58}Ni+^{58}Ni. This mass range of fragments is often taken for fitting the power law behavior of the mass yield ($\propto A_f^{-\tau}$). This power mass law dependence is also related to the liquid-gas phase transition, if any. Interestingly, the yields in all cases are steeper for the central collisions and lighter colliding nuclei. The slope becomes flat for peripheral collisions. Even the U-shape curve can be seen in some cases. This behavior seems to be independent of the system size as well as of the momentum correlations constraints. Further, all the mass yields can be nicely parametrized in terms of power laws $\propto A_f^{-\tau}$. The values of τ obtained for different reactions over different colliding geometry are summarized in Table I. From the table, we see that the value τ is independent of the mass of the colliding nuclei. Interestingly, for central collisions, it has a stronger impact on the momentum correlations whereas it is very little for the peripheral collisions. In all cases, the value of τ lies between 2 and 3. As has also been pointed out

TABLE I. The values of power factors τ for different reactions and impact parameters using MST and MSTP methods.

System	Method	$\hat{b} = 0.2$	$\hat{b} = 0.4$	$\hat{b} = 0.6$	$\hat{b} = 0.8$
^{12}C+^{12}C	MST	2.4±0.37	2.0±0.11	2.1±0.16	2.5±0.20
	MSTP	2.6±0.32	2.2±0.01	2.1±0.03	2.0±0.06
^{20}Ne+^{20}Ne	MST	2.2±0.39	2.1±0.13	2.3±0.13	2.7±0.11
	MSTP	2.4±0.32	2.2±0.03	2.2±0.01	2.4±0.02
^{40}Ca+^{40}Ca	MST	2.2±0.37	2.2±0.25	2.4±0.16	2.7±0.22
	MSTP	2.5±0.22	2.4±0.11	2.6±0.10	2.7±0.14
^{58}Ni+^{58}Ni	MST	2.3±0.38	2.2±0.30	2.4±0.27	2.8±0.29
	MSTP	2.6±0.30	2.4±0.09	2.5±0.08	2.9±0.16
^{93}Nb+^{93}Nb	MST	2.1±0.30	2.2±0.21	2.5±0.27	2.9±0.32
	MSTP	2.5±0.28	2.4±0.07	2.5±0.10	2.9±0.23
^{129}Xe+^{118}Sn	MST	2.3±0.40	2.3±0.30	2.6±0.41	2.9±0.53
	MSTP	2.5±0.31	2.5±0.21	2.8±0.32	2.8±0.12
^{139}La+^{139}La	MST	2.2±0.43	2.3±0.29	2.4±0.25	2.7±0.20
	MSTP	2.3±0.17	2.4±0.08	2.7±0.18	2.9±0.26
^{197}Au+^{197}Au	MST	2.2±0.39	2.2±0.27	2.5±0.34	2.7±0.38
	MSTP	2.5±0.31	2.4±0.15	2.6±0.17	2.8±0.20

in Ref. [15], the constraints of the momentum cut break the heavier fission products into intermediate mass fragments at peripheral collisions. These heavier fragments, however, are not considered for the power law behavior. Our present values of τ, though consistent with the predictions of liquid-gas phase transition, do not give a clear indication about the possible liquid-gas phase transitions in heavier nuclei. It is due to the fact that there is no unique dependence of τ on impact parameter. This is in agreement with the findings of Refs. [11,14]. The mass-independent behavior of the power yields in the spatial and spatial-momentum correlation methods is due to the fact that the light mass fragments emerge from the midrapidity region. Therefore, the effects such as surface, shadow of spectator matter as well as long-range Coulomb effects, which depend on the system size, are absent in these yields. This leads to the mass-independent behavior. Our results with impact parameter show similar trends as have been obtained for the ALADIN experiments for different colliding geometry [14] and also reported in theoretical studies [11]. In ALADIN experiments, one has considered ^{12}C+^{197}Au, ^{40}Ar+^{197}Au, and ^{58}Ni+^{197}Au reactions [14]. The fittings in the table have a dependence cA^{τ}. Though τ is quite close in MST and MSTP approaches, the c value has drastic variations. The difference in c using MST and MSTP methods can be as large as 76% therefore, it demands further investigation. We shall investigate individual fragments and their multiplicities within MST and MSTP methods and see how their relative production depends on the size of system and colliding geometry.

In Fig. 3, we display the relative effects of the momentum correlations over spatial correlations defined as

$$\Delta M_c\% = \left| \frac{(Mult)_{MSTP} - (Mult)_{MST}}{(Mult)_{MST}} \right| \%. \qquad (6)$$

Here, we display $\Delta M_c\%$ for A^{max}, the heaviest fragment, free nucleons, $A = 2$, $2 \leqslant A \leqslant 4$, $3 \leqslant A \leqslant 5$, $5 \leqslant A \leqslant 9$

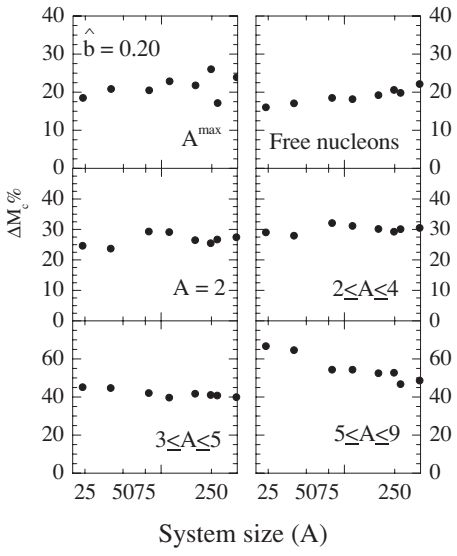

FIG. 3. The percentage difference $\Delta M_c\%$ as a function of the system size is displayed for A^{max}, free nucleons, $A = 2$, $2 \leqslant A \leqslant 4$, $3 \leqslant A \leqslant 5$, $5 \leqslant A \leqslant 9$, respectively.

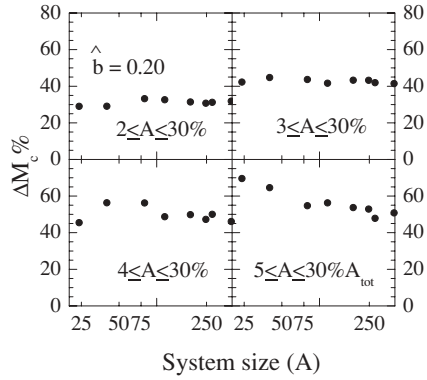

FIG. 4. Same as Fig. 3, but for $2 \leqslant A \leqslant 30\%$, $3 \leqslant A \leqslant 30\%$, $4 \leqslant A \leqslant 30\%$ of the heavier nuclei and $5 \leqslant A \leqslant 30\%$ of A_{tot}, respectively.

whereas all the intermediate mass fragments, i.e., fragments with masses $2 \leqslant A \leqslant 30\%$, $3 \leqslant A \leqslant 30\%$, $4 \leqslant A \leqslant 30\%$ of the heavier nuclei and $5 \leqslant A \leqslant 30\%$ of the A_{tot} are displayed in Fig. 4, for a typical $\hat{b} = 0.2$ colliding geometry. Very interestingly, a sizable and significant effect of momentum correlations can be seen in all types of fragments. It is also evident that the average effect of momentum correlations (when averaged over all fragments) is independent of the size of interacting nuclei. The average effect for central collisions ($\hat{b} = 0.2$) is $38.85 \pm 2.45\%$. This clearly suggests that one should include the momentum correlations cut in the clusterization process. This nearly mass-independent effect of the momentum correlations is due to the fact that the incident energy and colliding geometry was kept fixed while looking for the system-size effects. Once incident energy and impact parameter is fixed, the number of nucleon-nucleon collisions scales with the system size. In other words, one would expect a linear effect of momentum cut over system size. The observation of sizable effect of momentum correlations is significant since it has been pointed out in Ref. [17] that the ALADIN experimental data are underestimated by the MST method. The present enhancement due to momentum correlations can be helpful in this direction. Further, since effects exist for all masses, one should include momentum correlations in clusterization procedures.

Summarizing, we carried out a detailed study of the system-size effects and momentum correlations by simulating the reactions of ^{12}C+^{12}C, ^{20}Ne+^{20}Ne, ^{40}Ca+^{40}Ca, ^{58}Ni+^{58}Ni, ^{93}Nb+^{93}Nb, ^{129}Xe+^{118}Sn, ^{139}La+^{139}La, and ^{197}Au+^{197}Au at an incident energy of 400 MeV/nucleon and over an entire colliding geometry from central to extreme peripheral collisions. The mass yield can be parametrized in terms of the power law ($\propto A^{-\tau}$)with $2 \leqslant \tau \leqslant 3$ in all cases independent of the masses of colliding nuclei and impact parameter. Further, a mass-independent role of the momentum correlations over the entire periodic table was also obtained. When averaged over all fragments, the momentum correlations have an effect of about 39% over spatial correlations and are nearly independent of the system under consideration.

Work supported by CSIR, Government of India via grant no. 03(1078)/06/EMR-II, India.

[1] J. Aichelin and H. Stocker, Phys. Lett. **B176**, 14 (1986); J. Aichelin, Phys. Rep. **202**, 233 (1991).
[2] J. Singh and R. K. Puri, Phys. Rev. C **62**, 054602 (2000); R. K. Puri and S. Kumar, *ibid.* **57**, 2744 (1998); S. Kumar and R. K. Puri, *ibid.* **58**, 320 (1998).
[3] L. C. Vaz, J. M. Alexander, and G. R. Satchler, Phys. Rep. **69**, 373 (1981); R. K. Puri, Ph.D. thesis, Panjab University, Chandigarh (1990).
[4] A. D. Sood and R. K. Puri, Phys. Rev. C **69**, 054612 (2004).
[5] W. Reisdorf, Nucl. Phys. **A630**, 15c (1998).
[6] D. R. Bowman, *et al*., Phys. Rev. C **46**, 1834 (1992); E. Piasecki *et al*., Phys. Rev. Lett. **66**, 1291 (1991).
[7] C. Hartnack, J. Jaenicke, L. Sehn, H. Stocker, and J. Aichelin, Nucl. Phys. **A580**, 643 (1994).
[8] M. W. Curtin, H. Toki, and D. K. Scott, Phys. Lett. **123B**, 289 (1983).
[9] P. J. Siemens, Nature (London) **305**, 410 (1983), and references therein; P. Danielewicz, Nucl. Phys. **A314**, 465 (1979).
[10] M. E. Fisher, Rep. Prog. Phys. **30**, 615 (1967); D. Stauffer, Phys. Rep. **54**, 1 (1979).
[11] Y. G. Ma and W. Q. Shen, Phys. Rev. C **51**, 710 (1995); J. Pan and S. D. Gupta, *ibid.* **51**, 1384 (1995) ; T. Li *et al*., Phys. Rev. Lett. **70**, 1924 (1993).
[12] A. Insolia *et al*., Phys. Rev. C **61**, 044902 (1991).
[13] A. Bohnet *et al*., Phys. Rev. C **44**, 2111 (1995); G. Peilert *et al*., *ibid.* **39**, 1402 (1989).
[14] C. A. Ogilvie *et al*., Phys. Rev. Lett. **67**, 1214 (1991).
[15] J. K. Dhawan and R. K. Puri, Phys. Rev. C (to be published).
[16] S. Kumar and R. K. Puri, Phys. Rev. C **60**, 054607 (1999).
[17] M. Begemann-Blaich *et al*., Phys. Rev. C **48**, 610 (1993).